Transfer Learning Based Location-Aided Modulation Classification in Indoor Environments for Cognitive Radio Applications

K. TAMIZHELAKKIYA [1,3], Sabitha GAUNI [1,2], Prabhu CHANDHAR [3]

[1] Department of ECE, SRM Institute of Science and Technology, SRM Nagar, Kattankulathur, Chennai, Tamil Nadu, India
[2] Autosys Control Systems India Pvt Ltd, Chennai, Tamil Nadu, India
[3] Chandhar Research Labs Pvt Ltd, Chennai, Tamil Nadu, India

tk1045@srmist.edu.in, sabianup@gmail.com, prabhu@chandhar-labs.com

Submitted June 13, 2023 / Accepted August 12, 2023 / Online first October 30, 2023

Abstract. *Modulation classification is a crucial technique to utilize the unconsumed spectrum in Cognitive Radio (CR) and Dynamic Spectrum Access (DSA) systems to meet the required traffic demands for future-generation cellular networks. This paper presents an end-to-end experimental setup as a generic methodology to implement various Transfer Learning (TL) models in an indoor environment. This allows us to learn the features from multiple modulation signals to train and test the model. The performance evaluation of proposed TL models such as Convolutional Neural Network - Random Forest (CNN-RF), and Convolutional Long Short Term Deep Neural Network (CLDNN) - Random Forest (CLDNN-RF) have been thoroughly discussed. The result shows that the proposed TL models yield more than 90% classification accuracy for various modulation types. A proposed framework for location-specific TL model selection based on the maximum classification accuracy has been investigated.*

Keywords

Deep Learning (DL), modulation classification, CNN, Software Defined Radio (SDR), Transfer Learning (TL)

1. Introduction

Recently, utilizing the unconsumed spectrum of Cognitive Radio (CR) has become mandatory for telecom operators to meet next-generation traffic demands [1–3]. This leads to the expansion of enormous device connectivity with the 5G and beyond cellular networks [4] to support novel use cases such as smart cities, autonomous vehicles, smart factories, health care, and Internet-of-Things (IoT) applications [5]. Specifically, services providing Ultra Reliable Low Latency Communication (URLLC) for IoT devices have become predominant [6]. Thus, a paradigm shift is mandatory for the development of intelligent communication networks. The efficient usage of the spectrum is a promising solution to meet the current demands for next-generation networks. It can be achieved by using Dynamic Spectrum Access (DSA) along with CR technology [7]. In CR systems, the real-time samples must be periodically monitored in a wide range of frequency bands to detect inactive channels that can be reused further.

In DSA, Spectrum Sensing (SS) and power control have been utilized by the Secondary Users (SUs) to access the spectrum allocated to the Primary Users (PUs) [8]. It can be accomplished by continuously monitoring the modulation type used by the PUs. Once the modulation type is identified, the SU can adjust its transmit power, such that the interference of the PU is minimized. Thus, the modulation classification plays a significant role in CR to avoid interference between SU and PU [9]. Moreover, in DSA, modulation classification can be performed to detect and classify the interference sources and jammers coexisting within a wireless network [10]. The spectrum awareness at the edge device (mobile terminal) can also be performed via modulation classification. Moreover, future cellular systems are expected to support a billion devices for massive Machine Type Communication (mMTC). The massive devices create enormous implications on base stations at the expense of overhead and power consumption [11]. To meet these constraints and enhance the Quality of Service (QoS), CR-based Automatic Modulation Classification (AMC) systems have been developed with intelligent modems performing SS to effectively utilize the available radio spectrum.

In wireless communication systems, the modulation classification can be performed by a two-step process, namely, signal pre-processing and model generation methods. During signal pre-processing, the receiver performs noise reduction and parameter estimation of the received signal. The model generation process has been carried out by either Likelihood-based (LB) or feature-based (FB) method [12]. In [13], the primary features have been extracted by the traditional feature detection algorithms, then passed into the classifier system for signal classification.

DOI: 10.13164/re.2023.0531

Artificial Intelligence (AI) has emerged for thirty decades, which encompasses problem-solving machines in making decisions. Deep Learning (DL) / Transfer Learning (TL), is a category under AI that employs the most salient characteristic of feature learning in the decision process. The DL-based technique handles an enormous amount of data urged a need for automation in 5G and beyond cellular networks. The DL models, such as Convolution Neural Network (CNN) [14], Multi-Layer Perceptron (MLP) [15], Long Short Term Memory (LSTM) Network [16], Residual Network (ResNet) [17], Recurrent Neural Network (RNN), Convolutional and Long Short-Term Memory Deep Neural Network (CLDNN) [18], and ResNet+LSTM [19] have been developed to improve the AMC algorithms. In [20], the authors have compared the different types of input data formats for the modulation classification process and concluded that the I/Q format gives the best classification accuracy. In [21], the OFDM-based CNN model has been tested for BPSK, QPSK, 8PSK, and 16QAM. The different modulation waveforms ($\frac{\pi}{2}$-BPSK, QPSK, 16QAM, 64QAM, 256QAM) have been created using MATLAB 5G toolbox and classified by LeNet model under various channel conditions [22].

The ADAM-PLUTO and Universal Software Radio Peripherals (USRP) have been utilized to demonstrate the spectrum sharing in the CR systems [23] and achieve classification accuracies of 95.5% and 96.25% respectively. By using USRP captured signals, different DL methods such as a flexible Framework for Automatic Signal Classification Techniques (FACT) [24], and GNU architecture [25] have been analyzed for the classification of simultaneous Signals of Interests (SoIs), modulation, and Multi-sensor Modulation Classification (MMC) respectively.

There are four different TL approaches (Instances, feature representations, model parameters, and relational knowledge) for three types of TL techniques (Inductive [26], transductive [27], and unsupervised [28]). The instances approach re-weights some of the labeled data in the base model of the source domain to use in the new model of the target domain [29]. Feature representations find better feature characteristics that reduce the difference between the source/target domains and the misclassification rate. The model parameter discovers the coherence between the source/target domains and maps the relational knowledge between them [30]. A common practice of TL [31] is to adopt a trained model on a larger dataset and replace the Neural Network (NN) layer with Machine Learning (ML) classifier, then retrain the network using the smaller dataset for a specific task, such as plant leaf discrimination [32], fault diagnosis [33], and image recognition [34]. Moreover, the pre-defined CNN models have been formulated using an image dataset. We cannot adopt these models to develop the TL model by freezing the convolution layers for modulation classification tasks. To the best of the authors' concern, there is no pre-defined model systematized signal classification performance analysis. In this regard, we focus on the "with freezing" approach which remains the main scope of our research work. Here, we perform TL along with the features of the CNN model [35] and the NN classification part has been replaced by a Random Forest (RF) classifier.

The availability of excellent training datasets has limited many significant AI developments. We explored a huge amount of amazing datasets for the development of computer vision, modulation recognition, and Natural Language Processing (NLP). To recognize radio signals, there are numerous datasets available on an online platform. It has been noticed that the Graphics Processing Unit (GPU) is utilized to create the model which reduces the training overhead compared to Central Processing Unit (CPU). Moreover, Hisarmod2019.1 [36] and RadioML2018.10.a [37] are adopted with some channel impairments such as multipath fading and frequency offset. The datasets found in the literature may not be adequate for many practical situations. However, the simulation-based datasets may differ significantly with respect to real-world applications. From the literature work, we conclude that the real-world labeled training datasets with high quality are still lacking. Moreover, improvements in the accuracy of modulation classifying models for smaller sampling rates under different channel conditions in indoor environments have been found as a noteworthy problem.

The scope of environmental adaptation in TL is to adapt a learned model to a changing channel environment while maintaining the fixed transmitter/receiver pair(s). The factors such as channel type, any movement of the transmitter and/or receiver, sampling frequency offset, the selective fading may potentially create variations in signal capture which affect the learned behavior of a DL system. This motivates an indoor scenario of moving a transmitter/receiver pair equipped with an AMC model from a Line-of-Sight (LOS), Additive White Gaussian Noise (AWGN) channel to an environment with significant multipath effects and interference from the neighboring devices. The TL is a promising technology for realizing distributed learning techniques, where the propagation environment and hardware have a direct impact on the receiver AMC performance. In this paper, we investigate the TL models for modulation classification in indoor environments, since most of the devices in IoT, Machine-to-Machine (M2M), and Device-to-Device (D2D) applications are expected to be located indoors.

1.1 Contributions

The main contributions of our work are as follows:

- **Dataset preparation:** The traditional datasets are unrealistic for real-time environments, and cannot meet the expected performance. So far, no work has been found in the literature by varying the receiver positions for the fixed transmitter location. The experiments have been conducted in an indoor environment by changing the receiver positions for two fixed transmitter locations. We generate a Radio Frequency Signal Classification (RFSC) dataset for the adopted indoor channel model layout.

- **TL Model Generation/Verification:** We propose a novel TL-based Convolutional Neural Network-Random Forest (CNN-RF), and Convolutional Long Short Term Deep Neural Network (CLDNN) -Random Forest (CLDNN-RF) models using our own generated models such as CNN and CLDNN (CNN+LSTM) for modulation classification. The TL models have been generated by freezing the weights of convolutional layers in CNN; convolutional, and LSTM layers in CLDNN. Then, these features are fed into the RF classifier which improves the classification accuracy with minimal computational cost. Finally, the TL models have been evaluated using a testing dataset at different 50 receiver positions.

- **Domain adaptation based TL model selection:** The proposed TL-based domain adaptation method enhances the classification performance by adopting AWGN samples from the source domain and multipath samples from the target domain. The proposed method consists of a small-scale domain sub-network and is validated by Non-Line-of-Sight (NLOS) components which are generated from the open-source GNU platform. In the training dataset, there are LOS samples in the source and target domains. In the testing dataset, the NLOS samples from the target domain are used to simulate the real scenario. Finally, the Location-specific TL models have been selected/declared based on the highest classification accuracy between the different TL models for a given transmitter location and 50 receiver position of an indoor channel model.

The rest of this paper is organized as follows. The system model is presented in Sec. 2. In Sec. 3, we introduce our proposed TL models. In Sec. 4, simulation results are presented and discussed. Finally, this paper is concluded in Sec. 5.

2. System Model

We have developed an experimental setup for dataset preparation in real-time as shown in Fig. 1. We have chosen two SDRs, HackRF, and RTL-SDR for transmission and reception of different modulated waveforms using Deep Radio and Wi-Guy, respectively. Deep Radio is a transceiver device comprised of HackRF, a telescopic antenna, and GNU Radio. The major parameters such as carrier frequency, RF, IF, and base-band gains and bandwidth have been chosen for tuning the transmitter. The Wi-Guy receiver has been used to capture the real-time samples and Python language is used to process the baseband samples.

2.1 Transmitter: Signal Model

The signal transmitted from the Deep Radio is expressed as:

$$s(t) = \mathfrak{Re}\left\{A s_{\mathrm{b}}(t) \mathrm{e}^{\mathrm{j}2\pi f_{\mathrm{c}} t}\right\} \tag{1}$$

where A is amplitude, f_{c} is the carrier frequency and $s_{\mathrm{b}}(t)$ is an analog complex waveform, $s_{\mathrm{b}}(t) = \mathfrak{R}\{s_{\mathrm{b}}(t)\} + \mathrm{j}\mathfrak{I}\{s_{\mathrm{b}}(t)\}$ derived from the transmitter after modulating the discrete input bits (b_k). Hence, the resulting baseband signal $s(t)$ is real-valued with center frequency f_{c} to be transmitted, while $s_{\mathrm{b}}(t)$ base-band complex envelope of $s(t)$.

2.2 Receiver: Data Collection and Preprocessing

The systematic flow for model generation consists of data capturing, pre-processing, feature extraction, modulation classification, and a decision on trained models as shown in Fig. 2. The receiver captures the samples from the transmitter SDR. The received signal $r(t)$ is modelled as [20]:

$$r(t) = s(t) * h(t, \tau). \tag{2}$$

Here, $h(t, \tau)$ is a channel output described as a complex channel Finite Impulse Response (FIR) filter.

At the receiver, $r(t)$ is first down-converted and sampled at a rate $f_{\mathrm{s}} = \frac{1}{T_{\mathrm{s}}}$. The output of the Analog-to-Digital Converter (ADC) is given as:

$$r_{\mathrm{b}}[n] = r[nT_{\mathrm{s}}] = r_{\mathrm{b,I}}[n] + j r_{\mathrm{b,Q}}[n] \tag{3}$$

where $r_{\mathrm{b,I}}[n]$ and $r_{\mathrm{b,Q}}[n]$ are in-phase and quadrature-phase components, respectively.

In a single dataset, there are N samples collected over a time period of $T = NT_{\mathrm{s}}$ seconds. The complex raw samples $r_{\mathrm{b}}[n] \in \mathbb{C}$, $n = 0, 1, \ldots, N-1$, are represented in a data vector format. The k-th dataset vector of a collected input signal sample is denoted as:

$$\mathbf{r}_k = \left[r_{\mathrm{b}}[0], r_{\mathrm{b}}[1], \ldots, r_{\mathrm{b}}[N-1]\right]^{\mathrm{T}} \tag{4}$$

where T represents a transpose operation.

The samples are down-sampled by a factor D to reduce the sampling rate, which gives the resultant dataset as $r'_{\mathrm{b}}[m]$. It is represented as:

$$r'_{\mathrm{b}}[m] = r_{\mathrm{b}}[mD]. \tag{5}$$

The k-th dataset vector after decimation is denoted as:

$$\mathbf{r}'_k = \left[r'_{\mathrm{b}}[0], r'_{\mathrm{b}}[1], \ldots, r'_{\mathrm{b}}[N'-1]\right]^{\mathrm{T}} \tag{6}$$

where $N' = \frac{N}{D}$.

2.3 RF to Image Matrix Format Conversion

The decimated RF samples are fed into a matrix conversion block, which converts the samples into image format [38]. Let us denote the dataset for the m-th class as $\mathbf{r}'_{mk}$. The complex dataset vector $\mathbf{r}'_{mk} \in \mathbb{C}^{N'}$ is transformed into real valued data vectors $\mathbf{x}_{mk} \in 2N'$, namely, in-phase component ($r'_{\mathrm{b,I}}[m]$) and quadrature-phase component ($r'_{\mathrm{b,Q}}[m]$).

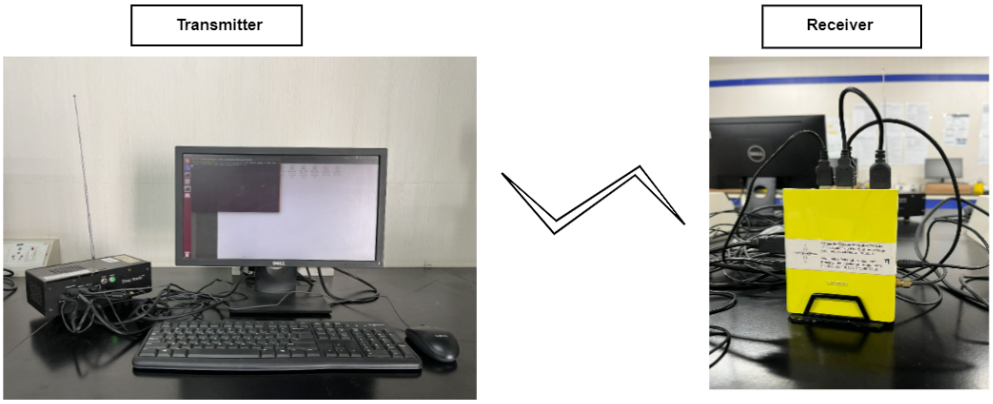

Fig. 1. Experimental setup for dataset preparation: Deep Radio transmitter, and Wi-Guy receiver.

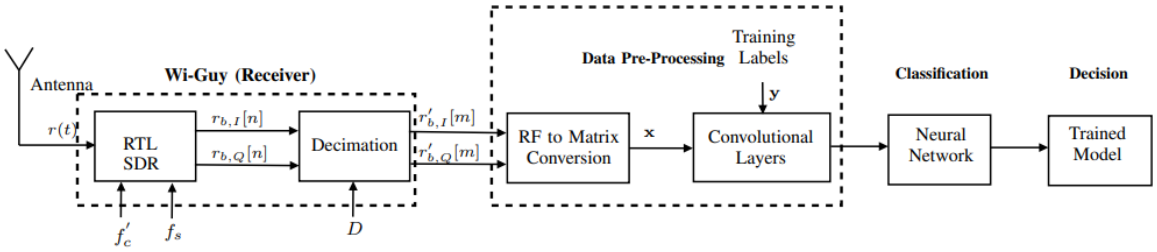

Fig. 2. Systematic flow of model generation and decision.

$$\mathbf{x}_{mk} = \left[\begin{pmatrix} r'_{\mathrm{b,I}}[0] & r'_{\mathrm{b,I}}[1] & \cdots & r'_{\mathrm{b,I}}[I_{\mathrm{W}}-1] \\ r'_{\mathrm{b,I}}[I_{\mathrm{W}}] & r'_{\mathrm{b,I}}[I_{\mathrm{W}}+1] & \cdots & r'_{\mathrm{b,I}}[2I_{\mathrm{W}}-1] \\ r'_{\mathrm{b,I}}[2I_{\mathrm{W}}] & r'_{\mathrm{b,I}}[2I_{\mathrm{W}}+1] & \cdots & r'_{\mathrm{b,I}}[3I_{\mathrm{W}}-1] \\ \vdots & \vdots & \vdots & \vdots \\ r'_{\mathrm{b,I}}[I_{\mathrm{H}-1}I_{\mathrm{W}}] & r'_{\mathrm{b,I}}[I_{\mathrm{H}-1}I_{\mathrm{W}}+1] & \cdots & r'_{\mathrm{b,I}}[I_{\mathrm{H}-1}I_{\mathrm{W}}-1] \end{pmatrix}_{I_{\mathrm{H}}\times I_{\mathrm{W}}}, \begin{pmatrix} r'_{\mathrm{b,Q}}[0] & r'_{\mathrm{b,Q}}[1] & \cdots & r'_{\mathrm{b,Q}}[I_{\mathrm{W}}-1] \\ r'_{\mathrm{b,Q}}[I_{\mathrm{W}}] & r'_{\mathrm{b,Q}}[I_{\mathrm{W}}+1] & \cdots & r'_{\mathrm{b,Q}}[2I_{\mathrm{W}}-1] \\ r'_{\mathrm{b,Q}}[2I_{\mathrm{W}}] & r'_{\mathrm{b,Q}}[2I_{\mathrm{W}}+1] & \cdots & r'_{\mathrm{b,Q}}[3I_{\mathrm{W}}-1] \\ \vdots & \vdots & \vdots & \vdots \\ r'_{\mathrm{b,Q}}[I_{\mathrm{H}-1}I_{\mathrm{W}}] & r'_{\mathrm{b,Q}}[I_{\mathrm{H}-1}I_{\mathrm{W}}+1] & \cdots & r'_{\mathrm{b,Q}}[I_{\mathrm{H}-1}I_{\mathrm{W}}-1] \end{pmatrix}_{I_{\mathrm{H}}\times I_{\mathrm{W}}} \right] \tag{7}$$

The k-th feature vector $\mathbf{x}_{mk}$ is given in (7). This k-th feature vector is further translated into a suitable matrix format to train the CNN model, $\mathbf{x}_{mk} \in \mathbb{R}^{I_{\mathrm{H}}\times I_{\mathrm{W}}\times I_{\mathrm{C}}}$ with size $(I_{\mathrm{H}} \times I_{\mathrm{W}} \times I_{\mathrm{C}})$, where I_{H} is the height, I_{W} is the width of an image, and I_{C} is the number of channels respectively. Here, $I_{\mathrm{H}}I_{\mathrm{W}}I_{\mathrm{C}} = 2N'$. Finally, the matrix $(\mathbf{x}_{mk})$ consists of in-phase $(r'_{\mathrm{b,I}}[m])$ and quadrature-phase $(r'_{\mathrm{b,Q}}[m])$ components that have been converted into the two images with a size of 28×28.

Let $\mathbf{x}_m \in \mathbb{R}^{K\times I_{\mathrm{H}}\times I_{\mathrm{W}}\times I_{\mathrm{C}}}$ be the dataset for the m-th class defined as a vector of K measurements (assume, $K = 500$ signals per modulation type) of m-th observation called as a feature vector:

$$\mathbf{x}_m = [\mathbf{x}_{m1}, \mathbf{x}_{m2}, \ldots, \mathbf{x}_{mK}]^{\mathrm{T}}, m = 1, 2, \ldots, M. \tag{8}$$

The entire input dataset is defined as:

$$\mathbf{X} = \begin{bmatrix} \mathbf{x}_1^{\mathrm{T}} \\ \mathbf{x}_2^{\mathrm{T}} \\ \vdots \\ \mathbf{x}_M^{\mathrm{T}} \end{bmatrix} \tag{9}$$

where M is the number of modulation types.

The multi-class label $\mathbf{y} \in R^M$ corresponding to M inputs $\mathbf{x}_m$, is denoted as:

$$\mathbf{y} = [y_1, y_2, \ldots, y_M]^{\mathrm{T}}, y_m \in 1, 2, \ldots, M. \tag{10}$$

Finally, the entire training dataset contains, M input-output pair that has been defined as:

$$S = \{(\mathbf{x}_1, y_1), (\mathbf{x}_2, y_2), \ldots, (\mathbf{x}_M, y_M)\}. \tag{11}$$

Here, each pair $(\mathbf{x}_m, y_m)$ represents a training sample that is used to train the CNN architecture for DL/TL model generation.

	Domain (D)	Elements (E)	Task (T)
Source (s)	D_s = a transmitter/receiver pair at a location one ($p1'$)	E_s = Rician channel, f_s = 2.4 MSps , Signal-to-Noise Ratio (SNR) = 6 to 10 dB	T_s= modulation classification
Target (t)	D_t = a single transmitter at TX2 and 50 different receiver positions ($p1'$–$p50'$)	E_t = Rayleigh channel, f_s = 2.4 MSps, multipath effects (NLOS components), SNR range = –5 to 5 dB	T_t= modulation classification, localization, model selection

Tab. 1. TL settings in RFML for environment adaptation domain.

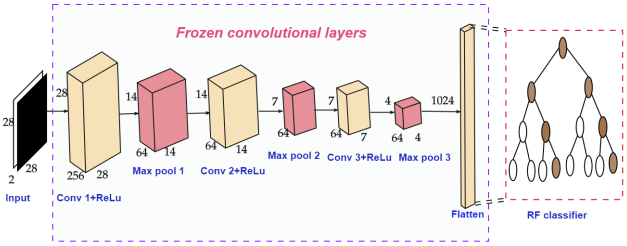

Fig. 3. CNN-RF model consists of frozen convolutional layers and the RF classifier.

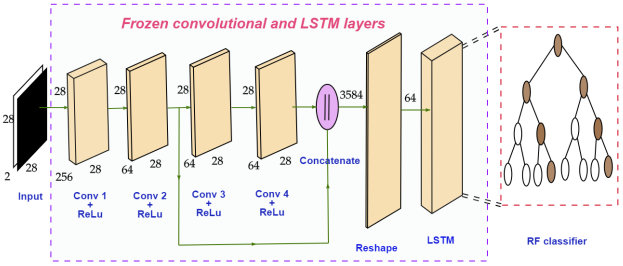

Fig. 4. CLDNN-RF model consists of four convolutional layers, one LSTM layer with the RF classifier.

3. Proposed TL Models

The notations of the TL are defined as: Domain $D = \{X, \mathrm{P}(X)\}$ consists of input data X and its marginal probabilities $\mathrm{P}(X)$, where $X = \{x_1, ..., x_n\} \in \chi$, where χ represents the input feature space and n is the number of observations. The task $T = \{Y, \mathrm{P}(Y|X)\}$ consists of label space Y and its conditional probabilities $\mathrm{P}(Y|X)$ learned from the data pairs $\{x_i, y_i\}$, where $x_i \in X$, and $y_i \in Y$ during the training process [29].

In our experiment, the D consists of SDRs and channel environment (building layout) to address the tasks (modulation classification, and model selection). The source domain (D_s=$\{X_s, \mathrm{P}(X_s)\}$) consists of elements (E_s) such as Ricean fading, bandwidth, and sampling rate to achieve the source task ($T_s = \{Y_s, \mathrm{P}(Y_s|X_s)\}$) as M-class modulation classification. Furthermore, the target domain (D_t= $\{X_t, \mathrm{P}(X_t)\}$) consists of the elements (E_t) such as multipath effects, and SNR to perform the target task $T_t = \{Y_t, \mathrm{P}(Y_t|X_t)\}$ as modulation classification, and model selection. The taxonomies used for the proposed TL model have been defined in Tab. 1. It has been observed that the receiver positions with 6 to 10 dB SNR experiences the Rician channel (E_s) and other SNR positions follow the Rayleigh channel with the presence of TX2 (E_t).

Traditional supervised ML techniques assume the criteria $D_s = D_t$ and $T_s = T_t$, for training the source domain (D_s) model to achieve modulation classification as a target task (T_t). In the context of Radio Frequency ML (RFML), implicit variations of TX/RX locations/positions and the channel effects guarantee that $D_s \neq D_t$, unlike Computer Vision (CV), and Natural Language Problem (NLP) applications. However, the TL is motivated by the mismatch between the source/target domains and tasks, which constrains the direct transfer between D_s, and D_t. Moreover, the scope of the TL is to leverage the knowledge $\mathrm{P}(Y_s|X_s)$ obtained using D_s and T_s to improve the performance of $\mathrm{P}(Y_t|X_t)$ on D_t and T_t. Here, we adopt the inductive TL because the source/target domains are having the labeled data. However, the different source/target data distributions and the feature spaces can be caused by either a change in hardware (Deep Radio/Wi-Guy) or a change in the environment platform (with TX1/TX2).

In our proposed work, we consider the source/target tasks are the same, but the source/target domains may differ. Hence, we conduct an environmental domain adaptation approach with the same hardware device tested at two different transmitter locations, and 50 receiver positions. Here, a base DL model for CNN is generated by using a base dataset operated with TX1 alone (D_s) to perform modulation classification in the Rician/AWGN channel (T_s). Then, the trained network weights have been reused in the proposed TL models (CNN-RF, CLDNN-RF) with a new dataset generated with TX2 alone (D_t) to perform modulation classification in a fading channel (T_t) environment.

A significant amount of knowledge has been transferred from the base network to the newly designed network. This can be achieved with/without freezing the layers of the network. In order to reduce the computational complexity, we have frozen the convolutional layers of CNN, and CLDNN base model [35], where the weights/features from the convolutional layers have been directly passed to the RF classifier to create a novel TL model that performs the modulation classification as shown in Fig. 3 and 4 respectively. The RF classifier performs well on input features presented in tabular format rather than the raw samples. The RF classifier contains multiple decision trees and the output has been calculated based on the ensemble of decision trees to improve the predictive accuracy of the dataset.

4. Results and Discussion

Extensive measurements have to be performed to create the RFSC dataset for modulation classification under confined space. We create a measurement setup consisting of the SDR-based indoor modulation classification system using a single TX location and multiple RX positions (p).

The basic concept and part of the dataset have been obtained from our previous measurements [35]. In this section, the whole measurement procedure for an indoor environment has been described in detail.

4.1 Measurement Layout

The measurement has been carried out within the indoor scenario of Chandhar Research Labs Pvt Ltd, Chennai, India (Lat:13.08012, Lon:80.22857). The building dimension $430 \times 363 \times 235$ (inches) located on the ground floor of the complex. It consists of three lab portions (each has nine RX positions), one office room (nine RX positions), one kitchen (five RX positions), and a hall (nine RX positions) in the layout. The office portion is made up of concrete walls lined up with plasterboard and the ceiling material with a paint finish. This also includes wood cabinets, windows, several chairs, two tables, computers, and one desk. However, there are two transmitter locations in two different labs and 50 varying receiver positions spread across the building layout [35]. The dataset is available for download from https://www.kaggle.com/datasets/chandharlabs/rfsc-dataset. The simulation and signal parameters such as modulation type, sampling rate, carrier frequency, and SNR adopted for conducting the experiments are shown in Tab. 2.

For each modulation type, we have generated 1,500 and 500 samples for training and testing cases. Further, the training dataset (10,500 samples) has been divided into 7350 and 3150 samples (70:30), for model training and validation, respectively. It has been noticed that the models are generated from the samples collected at locations very close to the transmitter. In the presence of TX1 and $p1'$ (position $1'$), we generate the base CNN and CLDNN models. The model weights and bias values are frozen and fed into the RF classifier which generates two TL models (CNN-RF and CLDNN-RF). The performance of the model has been verified from a LOS (AWGN/Rician) to a multipath environment (TX2) with significantly 50 varying receiver positions.

Parameter	Value
Transmit power (p_t)	10 dBm
TX antenna	Telescopic antenna
Operating frequency range of transmitter	50 MHz to 6 GHz
TX antenna gain	0 dB
RX antenna	Whip antenna
Operating frequency range of receiver	50 MHz to 950 MHz
RX antenna gain	0 dB
Carrier frequency (f_c)	810 MHz
Receiver sampling frequency (f_s)	2.4 MSps
SNR range	–5 to 10 dB
Decimation factor (D)	12
Input image size ($I_H \times I_W \times I_C$)	$28 \times 28 \times 2$
Number of signals per class (K)	500
Training and testing ambience	i5 CPU,Tensorflow+Keras
Samples in training dataset	10,500
Samples in testing dataset	3,500

Tab. 2. Simulation parameters used for model generation and validation.

The entire process of the location-aided modulation classification technique has been described in Algorithm 1. The dataset preparation, training, and testing codes are available here: https://github.com/Tamizhelakkiya/Location-aided-TL-model.

Algorithm 1. A TL based location aided modulation classification for indoor scenario.

Input: RFSC Dataset (D), No. of Convolutional layers (l), No. of trees in RF (n)
RF to Image conversion: Convert the RFSC I/Q dataset ($r_b[n] = r_{b,I}[n] + j\, r_{b,Q}[n]$) into RFSC Image Dataset
for $p = 1$ to 50 **do**
  for $m = 1$ to 7 **do**
    1. Take k^{th} complex dataset vector : $\mathbf{r}_{mk} \in C^N$
    2. Transform complex data vectors into real-valued data vectors $\mathbf{x}_{mk} \in 2N$
    3. Translate $\mathbf{x}_{mk}$ into matrix format, $R^{I_H \times I_W \times I_C}$
    4. Convert $\mathbf{x}_{mk}$ into images (I).
  end for
end for
Parameters: $I = (x_1, y_1), (x_2, y_2), \ldots, (x_N, y_N)$, training images (Xtrain) and its labels (Ytrain), no. of receiver positions (p), and no. of transmitter locations (TX)
Define TL models:
while $TX = 2$ **do**
  1. Creates a model object of the Keras Model class with required input and output.
  2. Freeze the convolutional layers of CNN and CLDNN model [35] for feature extraction.
  3. Define the Random Forest Classifier architecture.
  4. Specify loss function, optimizer type, and metrics.
  5. Train and save the TL-model.
  6. TL models (CNN-RF, CLDNN-RF) have been generated.
end while
for $p = 1$ to 50 **do**
  Calculate classification accuracy

$$\mathbf{A}(\%) = \frac{\sum_{i=1}^{M} (\hat{y}_i == y_i)}{\sum_{i=1}^{M} y_i} \times 100\%.$$

  Identify the positions with $\mathbf{A} \geq 90\%$ and count the positions for each modulation type.
  Location aided modulation classification using CNN-RF, CLDNN-RF:
  for $SNR = -5$ to 4 **do**
    Classification accuracy($\mathbf{A}$)= CLDNN-RF[p]
    for $SNR = 5$ to 10 **do**
      Classification accuracy($\mathbf{A}$)= CNN-RF[p]
    end for
  end for
end for
Output: Classification accuracy ($\mathbf{A}$)

Model	Layers	Learnable parameters	Model generation time (minutes)
CNN [35]	6	3,21,415	15
CNN-RF	4	1,89,312	8.5
CLDNN [35]	9	11,69,607	65
CLDNN-RF	6	11,60,384	25.97

Tab. 3. Comparison of model size, learning parameters, and training time between DL/TL models.

Table 3 compares the number of parameters and model generation time for various DL/TL architectures. The model generation time has been found to be moderate for CNN-RF and CLDNN-RF models. It has been observed that CNN-RF possesses the least number of learnable parameters with reduced model size due to the freezing mechanism. Moreover, the CLDNN-RF behaves similarly to the CLDNN model for the learnable parameters with reduced model size and generation time.

4.2 Confusion Matrix

The confusion matrices for the proposed TL models at receiver position two, in the presence of TX2, are shown in Fig. 5. The probability values in each grid represent the classification accuracy of each modulation type. It has been observed that the CNN-RF model provides improved performance, particularly for BPSK, CPFSK, GFSK, and 16QAM modulation schemes. Moreover, the misclassification rate among different modulation classes was found to be reduced for the predicted labels. The CLDNN-RF model achieves the best classification score for 64QAM, QPSK, and GMSK. It has been noticed CNN-RF and CLDNN-RF provide better performance for low SNR positions.

4.3 Positions Count Based on 90% Classification Rate

Table 4 shows the position count where the average classification is more than 90% for all four models. Under locations TX1 and TX2, particularly in the case of GFSK, QPSK, and CPFSK modulation types, CNN-RF and CLDNN-RF provide similar performance. For 16QAM and GMSK, the CLDNN-RF provides better position counts. It has been found that the GFSK modulation type has been well classified in more position counts by proposed TL models compared with pre-trained CNN models. Furthermore, it has been observed that the proposed TL models provide $\geq$ 90% accuracy for more than 30 positions in the adopted building layout for all seven modulation types.

4.4 Location Specific TL Model Selection

In this section, we propose a location-aided TL strategy to perform the modulation classification for a given location. In this context, we perform an environment adaptation that adapts a learned model to a changing environment, while maintaining a fixed transmitter/receiver pair. The framework illustrates a varying transmitter (TX location)/receiver (RX position) pair equipped with the TL model from a single room to an entire building layout as shown in Fig. 6. For the source domain/task, the dataset has been tested for the proposed models and the model files have been generated using training data from the source domain (D_s).

The best TL model can be selected at each receiver position based on the highest classification accuracy adapting to the proposed indoor environment domain. Then, the weights

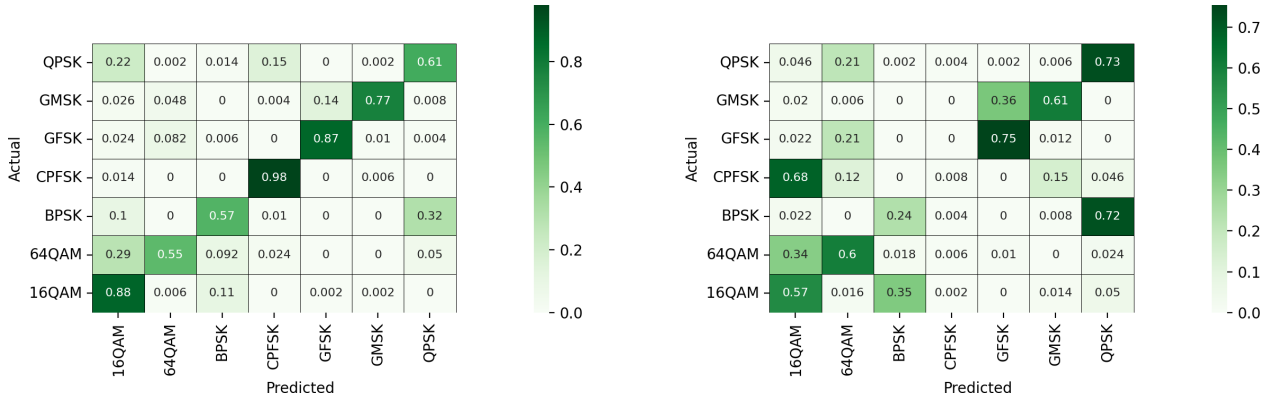

(a) CNN-RF model (b) CLDNN-RF model

Fig. 5. Confusion matrices of proposed TL models (CNN-RF, and CLDNN-RF) at receiver position two with transmitter location TX2.

Modulation Type →	**16QAM**		**64QAM**		**BPSK**		**CPFSK**		**GFSK**		**GMSK**		**QPSK**	
Model ↓	**TX1**	**TX2**	**TX1**	**TX2**	**TX1**	**TX2**	**TX1**	**TX2**	**TX1**	**TX2**	**TX1**	**TX2**	**TX1**	**TX2**
CLDNN [35]	24	33	20	28	20	16	18	10	17	15	19	31	30	34
CNN [35]	20	33	17	14	20	9	29	23	1	1	32	37	33	37
ResNet [35]	22	34	19	17	24	19	23	21	19	11	30	36	27	27
CNN-RF	30	34	32	31	33	30	31	31	32	30	38	35	39	38
CLDNN-RF	38	36	32	33	31	33	30	32	32	30	38	37	38	39

Tab. 4. Position count for various DL/TL models based 90% classification rate with two transmitter locations.

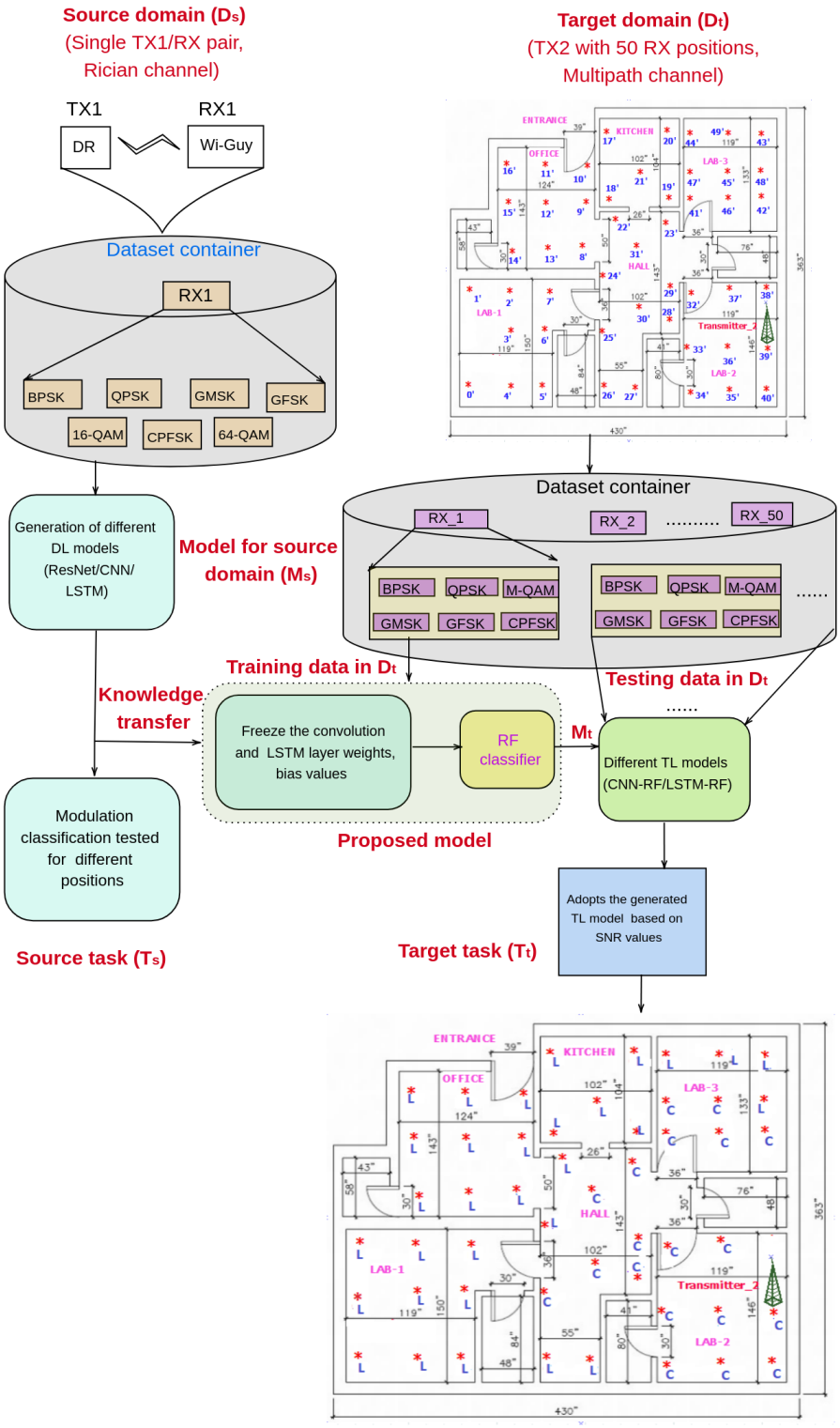

Fig. 6. Proposed framework for location-aided modulation classification consists of source/target domain. Here, L, and C represents CLDNN-RF, and CNN-RF model respectively.

and bias values passing through the frozen layers of CNN, and CLDNN [35] models (M_s) have been transferred to the target domain (D_t). The parameters of the RF classifier are continually trained using data from the target domain and the model (M_t) can be learned. Here, we assume the TX1 and TX2 locations are situated at LAB-1 (Between $p0'$ and $p1'$), and LAB-2 (between $p38'$ and $p39'$) respectively. We also verified that the receiver positions ($p32'$–$p40'$) experience the Rician channel and the remaining positions follow the Rayleigh channel with the presence of TX2.

Each receiver position in T_t estimates the SNR value for the transmitter (TX2) located at LAB-2, which is situated 10 m away from TX1. Based on the generated DL models, the gained knowledge obtained from TX1 (LOS (AWGN/Rician) has been transferred to multipath TX2 with significantly 50 varying receiver positions. From the received SNR, it adopts either CNN-RF/CLDNN-RF model to perform modulation classification. Here, the notations: L and C represent CLDNN-RF and CNN-RF models, respectively. It has been observed that the source/target task has been accomplished by the dataset generated at TX1, and TX2 locations with different receiver positions respectively. Moreover, we found that an incredible feature of TL improves the number of receiver positions where the modulation classification accuracy is above 90%.

Furthermore, we identified that the CNN-RF model has been selected in dominant Rician fading channel positions and the CLDNN-RF model for Rayleigh fading channel positions. We noticed that with transmitter location TX2; L, and C models provide the best classification performance with a count of 31 (SNR: –5 to 5 dB), and 19 (SNR: 5 to 10 dB) receiver positions, respectively. Finally, we conclude that the TL designer can select either CNN-RF (C) or CLDNN-RF (L) model based on indoor channel conditions.

4.5 Comparison of Model Performance using RFSC Dataset

In this section, we tested various CNN models generated for the RFSC dataset using GNU Radio which includes a variety of channel impairments such as fading, frequency offset, and sample rate offset. We have analyzed the model performance for the SNR range varying between –5 dB to 10 dB. From Fig. 7, we noticed that the classification accuracies of the generated models increase gradually with the progress of SNR values.

We have found that the highest accuracy has been achieved by the proposed TL models in most cases of SNR values. The peak accuracy achieved by the proposed TL models has been found to be efficient even in low SNR values. Moreover, we can observe that the classification accuracy is $\geq$ 90% at 2 dB. In the case of the multipath fading environment at $p1'$–$p30'$, the received signals experiencing lower and medium SNRs, the proposed TL models double the improvements in classification accuracies than the adopted

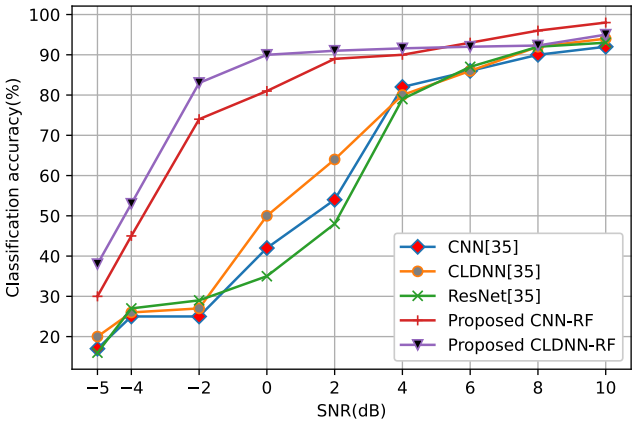

Fig. 7. Comparison of classification accuracy for various DL/TL models generated using RFSC dataset.

models below 4 dB SNR values. In the case of high SNR scenarios, particularly above 8 dB, all the models converge to provide the same performance.

5. Conclusion

In this paper, we presented a novel TL-based modulation classification task that is necessary for the DSA and CR systems. Our approach revolves around an end-to-end experimental setup for preparing the RFSC dataset to classify the modulation types by incorporating the effects of two fixed transmitter locations and 50 varying receiver positions for a given indoor environment. The proposed TL-based CNN-RF and CLDNN-RF models provide better classification performance than the other pre-trained models. Furthermore, the position counts based on a 90% classification rate have been discussed. We also presented a framework for location-specific TL model selection based on the maximum classification accuracy. This work can also be extended for novel algorithms to address modulation classes adopted for 5G and beyond systems.

Finally, we conclude our approach emerged as a good envision for Deep Learning/signal processing professionals, wireless engineers, and industry partners to design infrastructure for next-generation technologies IoT, M2M, D2D, and smart cities that address data-related issues with respect to cross-technology co-existence, ineffective spectrum utilization, and traffic regulation.

References

[1] AKYILDIZ, I. F., KAK, A., NIE, S. 6G and beyond: The future of wireless communications systems. *IEEE Access*, 2020, vol. 8, p. 133995–134030. DOI: 10.1109/ACCESS.2020.3010896

[2] LETAIEF, K. B., CHEN, W., SHI, Y., et al. The roadmap to 6G: AI-empowered wireless networks. *IEEE Communications Magazine*, 2019, vol. 57, no. 8, p. 84–90. DOI: 10.1109/MCOM.2019.1900271

[3] ALSHARIF, M. H., KELECHI, A. H., ALBREEM, M. A., et al. Sixth generation (6G) wireless networks: Vision, research activities, challenges, and potential solutions. *Symmetry*, 2020, vol. 12, no. 4. DOI: 10.3390/sym12040676

[4] AKHTAR, T., TSELIOS, C., POLITIS, I. Radio resource management: Approaches and implementations from 4G to 5G and beyond. *Wireless Networks*, 2021, vol. 27, no. 1, p. 693–734. DOI: 10.1007/s11276-020-02479-w

[5] CHETTRI, L., BERA, R. A comprehensive survey on Internet of Things (IoT) toward 5G wireless systems. *IEEE Internet of Things Journal*, 2020, vol. 7, no. 1, p. 16–32. DOI: 10.1109/JIOT.2019.2948888

[6] JI, H., PARK, S., YEO, J., et al. Ultra-reliable and low-latency communications in 5G downlink: Physical layer aspects. *IEEE Wireless Communications*, 2018, vol. 25, no. 3, p. 124–130. DOI: 10.1109/MWC.2018.1700294

[7] CHALLITA, U., SANDBERG, D. Deep reinforcement learning for dynamic spectrum sharing of LTE and NR. In *Proceedings of the IEEE International Conference on Communications*. Montreal (QC, Canada), 2021, p. 1–6. DOI: 10.1109/ICC42927.2021.9500325

[8] TSAKMALIS, A., CHATZINOTAS, S., TERSTEN, B. Automatic modulation classification for adaptive power control in cognitive satellite communications. In *Proceedings of the 7th Advanced Satellite Multimedia Systems IEEE Conference and the 13th Signal Processing for Space Communications Workshop (ASMS/SPSC)*. Livorno (Italy), 2014, p. 234–240. DOI: 10.1109/ASMS-SPSC.2014.6934549

[9] POLAK, L., KALLER, O., KLOZAR, L., et al. Influence of mobile network interfering products on DVB-T/H broadcasting services. In *Proceedings of the IFIP Wireless Days*. Dublin (Ireland), 2012, p. 1–5. DOI: 10.1109/WD.2012.6402860.

[10] SHI, Y., DAVASLIOGLU, K., SAGDUYU, Y. E., et al. Deep learning for RF signal classification in unknown and dynamic spectrum environments. In *Proceedings of the IEEE International Symposium on Dynamic Spectrum Access Networks (DySPAN)*. Newark (NJ, USA), 2019, p. 1–10. DOI: 10.1109/DySPAN.2019.8935684

[11] TENG, C.-F., CHOU, C.-Y., CHEN, C.-H., et al. Accumulated polar feature-based deep learning for efficient and lightweight automatic modulation classification with channel compensation mechanism. *IEEE Transactions on Vehicular Technology*, 2020, vol. 69, no. 12, p. 15472–15485. DOI: 10.1109/TVT.2020.3041843

[12] HATZICHRISTOS, G., FARGUES, M. P. A hierarchical approach to the classification of digital modulation types in multipath environments. In *Proceedings of the Conference Record of Thirty-Fifth Asilomar Conference on Signals, Systems and Computers*. Pacific Grove (CA, USA), 2001, p. 1494–1498. DOI: 10.1109/ACSSC.2001.987737

[13] KIM, K., AKBAR, I. A., BAE, K., et al. Cyclostationary approaches to signal detection and classification in cognitive radio. In *Proceedings of the IEEE International Symposium on New Frontiers in Dynamic Spectrum Access Networks (DySPAN)*. Dublin (Ireland), 2007, p. 212–215. DOI: 10.1109/DYSPAN.2007.35

[14] TURCANIK, M., PERDOCH, J. SAMPLE dataset objects classification using deep learning algorithms. *Radioengineering*, 2023, vol. 32, no. 1, p. 63–73. DOI: 10.13164/re.2023.0063

[15] EBRAHIMZADEH, A., GHAZALIAN, R. Blind digital modulation classification in software radio using the optimized classifier and feature subset selection. *Engineering Applications of Artificial Intelligence*, 2011, vol. 24, no. 1, p. 50–59. DOI: 10.1016/j.engappai.2010.08.008

[16] CHEN, Y., SHAO, W., LIU, J., et al. Automatic modulation classification scheme based on LSTM with random erasing and attention mechanism. *IEEE Access*, 2020, vol. 8, p. 154290–154300. DOI: 10.1109/ACCESS.2020.3017641

[17] JIA, F., YANG, Y., ZHANG, J., et al. A hybrid attention mechanism for blind automatic modulation classification. *Transactions on Emerging Telecommunications Technologies*, 2022, vol. 33, no. 7, p. 1–18. DOI: 10.1002/ett.4503

[18] PIJACKOVA, K., GOTTHANS, T. Radio modulation classification using deep learning architectures. In *Proceedings of the 31st IEEE International Conference Radioelektronika (RADIOELEKTRONIKA)*. Brno, (Czech Republic), 2021, p. 1–5. DOI: 10.1109/RADIOELEKTRONIKA52220.2021.9420195

[19] ELSAGHEER, M. M., RAMZY, S. M. Hybrid model for automatic modulation classification based on residual neural networks and long short term memory. *Alexandria Engineering Journal*, 2023, vol. 67, p. 117–128. DOI: 10.1016/j.aej.2022.08.019

[20] KULIN, M., KAZAZ, T., MOERMAN, I., et al. End-to-end learning from spectrum data a deep learning approach for wireless signal identification in spectrum monitoring applications. *IEEE Access*, 2017, vol. 6, p. 18484–18501. DOI: 10.1109/ACCESS.2018.2818794

[21] SHI, J., HONG, S., CAI, C., et al. Deep learning-based automatic modulation recognition method in the presence of phase offset. *IEEE Access*, 2020, p. 1–10. DOI: 10.1109/ACCESS.2020.2978094

[22] ALHAZMI, M. H., ALYMANI, M., ALHAZMI, H., et al. 5G signal identification using deep learning. In *Proceedings of the Wireless and Optical Communications Conference (WOCC)*. Newark (NJ, USA), 2020, p. 1–5. DOI: 10.1109/WOCC48579.2020.9114912

[23] GRAVELLE, C., ZHOU, R. SDR demonstration of signal classification in real-time using deep learning. In *Proceedings of the IEEE Globecom Workshops (GC Wkshps)*. Waikoloa (HI, USA), 2019, p. 1–5. DOI: 10.1109/GCWkshps45667.2019.9024661

[24] JAGANNATH, J., SAARINEN, H. M., DROZDA, L. Framework for automatic signal classification techniques (FACT) for software-defined radios. In *Proceedings of the IEEE Symposium on Computational Intelligence for Security and Defense Applications (CISDA)*. Verona (NY, USA), 2015, p. 1–7. DOI: 10.1109/CISDA.2015.7208628

[25] BJORSELL, N., VITO, L., RAPUANO, S. A GNU radio-based signal detector for cognitive radio systems. In *Proceedings of the IEEE International Instrumentation and Measurement Technology Conference*. Hangzhou, (China), 2011, p. 1–5. DOI: 10.1109/IMTC.2011.5944235

[26] CRAWFORD, M., KHOSHGOFTAAR, T. M. Using inductive transfer learning to improve hotel review spam detection. In *Proceedings of the 22nd International Conference on Information Reuse and Integration for Data Science (IRI)*. Las Vegas (NV, USA), 2021, p. 248–254. DOI: 10.1109/IRI51335.2021.00040

[27] MOREO, A., ESULI, A., SEBASTIANI, F. Lost in transduction: Transductive transfer learning in text classification. *ACM Transactions on Knowledge Discovery from Data*, 2021, vol. 16, no. 1, p. 1–21. DOI: 10.1145/3453146

[28] COHN, R., HOLM, E. Unsupervised machine learning via transfer learning and k-means clustering to classify materials image data. *Integrating Materials and Manufacturing Innovation*, 2021, vol. 10, no. 2, p. 231–244. DOI: 10.1007/s40192-021-00205-8

[29] PAN, S. J., YANG, Q. A survey on transfer learning. *IEEE Transactions on Knowledge and Data Engineering*, 2010, vol. 22, no. 10, p. 1345–1359. DOI: 10.1109/TKDE.2009.191

[30] ZHUANG, F., QI, Z., DUAN, K., et al. A comprehensive survey on transfer learning. *Proceedings of the IEEE*, 2021, vol. 109, no. 1, p. 43–76. DOI: 10.1109/JPROC.2020.3004555

[31] BU, K., HE, Y., JING, X., et al. Adversarial transfer learning for deep learning based automatic modulation classification. *IEEE Signal Processing Letters*, 2020, vol. 27, p. 880–884. DOI: 10.1109/LSP.2020.2991875

[32] MOYAZZOMA, R., HOSSAIN, M. A. A., ANUZ, M. H., et al. Transfer learning approach for plant leaf disease detection using CNN with pre-trained feature extraction method Mobilnetv2. In *Proceedings of the 2nd International Conference on Robotics, Electrical and Signal Processing Techniques (ICREST)*. Dhaka, (Bangladesh), 2021, p. 526–529. DOI: 10.1109/ICREST51555.2021.9331214

[33] MA, P., ZHANG, H., FAN, W., et al. A novel bearing fault diagnosis method based on 2D image representation and transfer learning-convolutional neural network. *Measurement Science and Technology*, 2019, vol. 30, no. 5, p. 1–16. DOI: 10.1088/1361-6501/ab0793

[34] BANSAL, M., KUMAR, M., SACHDEVA, M., et al. Transfer learning for image classification using VGG19: Caltech-101 image data set. *Journal of Ambient Intelligence and Humanized Computing*, 2021, vol. 14, p. 3609–3620. DOI: 10.1007/s12652-021-03488-z

[35] TAMIZHELAKKIYA, CHANDHAR, P., GAUNI, S. Comparison of deep architectures for indoor RF signal classification. In *Proceedings of the International Conference on Emerging Techniques in Computational Intelligence (ICETCI)*. Hyderabad (India), 2021, p. 107–112. DOI: 10.1109/ICETCI51973.2021.9574083

[36] ZHOU, Q., ZHANG, R., ZHANG, F., et al. An automatic modulation classification network for IoT terminal spectrum monitoring under zero-sample situations. *EURASIP Journal on Wireless Communications and Networking*, 2022, vol. 2022, no. 1, p. 1–18. DOI: 10.1186/s13638-022-02099-2

[37] O'SHEA, T. J., WEST, N. Radio machine learning dataset generation with GNU radio. *Proceedings of the 6th GNU Radio Conference*, 2016, vol. 1, no. 1, p. 1–6. [Online] Available at: https://pubs.gnuradio.org/index.php/grcon/article/view/11

[38] LIN, Y., TU, Y., DOU, Z., et al. Contour stella image and deep learning for signal recognition in the physical layer. *IEEE Transactions on Cognitive Communications and Networking*, 2021, vol. 7, no. 1, p. 34–46. DOI: 10.1109/TCCN.2020.3024610

About the Authors . . .

K. TAMIZHELAKKIYA received her B.E (ECE) degree from Periyar Maniammai College of Technology for Women, Tamil Nadu, India in 2008, and her M.E (Communication Systems) degree from Dhanalakshmi Srinivasan Engineering College, Tamil Nadu, India in 2011. Currently, she is perusing a Ph.D. degree in Wireless Communication at SRM Institute of Science and Technology, Chennai, India. Since 2020, she is working as a Wireless Researcher at Chandhar Research Labs, Chennai, India. Her research interests are signal processing and deep learning techniques for wireless communication systems.

Sabitha GAUNI (corresponding author) received a Ph.D. degree in Wireless Communication, in 2015. Presently, she serves as the Director of Autosys Control Systems India Pvt. Ltd, Chennai, India. From 2004 to 2022 she has been with the Dept. of ECE, SRM Institute of Science and Technology, Kattankulathur, India, as an Associate Professor. She has four patents to her credit. She has published several papers in refereed journals. Her research interests include wireless communication, signal processing, optical communication, and image processing. She is a member of several professional societies, such as IEEE, IEI, IETE, OSI, and ISTE.

Prabhu CHANDHAR received the Ph.D. degree from IIT Kharagpur, Kharagpur, India. From 2009 to 2010, he was a Senior Research Fellow at the Vodafone IIT KGP Centre of Excellence in Telecommunications, IIT Kharagpur. From 2015 to 2017, he was a Post-Doctoral Researcher at the Division of Communication Systems, Linköping University, Linköping, Sweden. Since 2018, he serves as the Director of Chandhar Research Labs, Chennai, India. His research interests are within the fields of signal processing and communication theory.